Cardiac tissue geometry as a determinant of unidirectional conduction block: assessment of microscopic excitation spread by optical mapping in patterned cell cultures and in a computer model

Vladimir G Fast and André G Kléber

Objective: Unidirectional conduction block (UCB) and reentry may occur as a consequence of an abrupt tissue expansion and a related change in the electrical load. The aim of this study was to evaluate critical dimensions of the tissue necessary for establishing UCB in heart cell culture. **Methods:** Neonatal rat heart cell cultures with cell strands of variable width emerging into a large cell area were grown using a technique of patterned cell growth. Action potential upstrokes were measured using a voltage sensitive dye (RH-237) and a linear array of 10 photodiodes with a 15 μm resolution. A mathematical model was used to relate action potential wave shapes to underlying ionic currents. **Results:** UCB (block of a single impulse in anterograde direction – from a strand to a large area – and conduction in the retrograde direction) occurred in narrow cell strands with a width of 15(SD 4) μm (1-2 cells in width, $n = 7$) and there was no conduction block in strands with a width of 31(8) μm ($n = 9$, $P < 0.001$) or larger. The analysis of action potential waveshapes indicated that conduction block was either due to geometrical expansion alone ($n = 5$) or to additional local depression of conduction ($n = 2$). In wide strands, action potential upstrokes during anterograde conduction were characterised by multiple rising phases. Mathematical modelling showed that two rising phases were caused by electronic current flow, whereas local ionic current did not coincide with the rising portions of the upstrokes. **Conclusions:** (1) High resolution optical mapping shows multiphasic action potential upstrokes at the region of abrupt expansion. At the site of the maximum decrement in conduction, these peaks were largely determined by the electrotonus and not by the local ionic current. (2) Unidirectional conduction block occurred in strands with a width of 15(4) μm (1-2 cells).

Cardiovascular Research 1995;**29**:697-707

Formation of unidirectional conduction block (UCB) is the initiating event in reentrant arrhythmias. It has been proposed that three principal mechanisms are responsible for unidirectional block. (1) The spatial dispersion of refractoriness in closely adjacent membrane sites may cause block of excitation.[1-3] This type of block depends on the delivery of a critically timed premature stimulus or on rapid pacing. (2) UCB may result from asymmetrical depression of excitability. This type of block was shown in isolated Purkinje fibres with asymmetrically applied pressure or cooling[4] and in one-dimensional computer models of cardiac excitation.[5 6] (3) UCB may occur as a consequence of the asymmetrical structure of cardiac tissue and the related change in electrical load. Such a mechanism was first demonstrated in a one-dimensional model of an axon with increasing diameter[7 8] or branching.[9] Later it was shown in a computer model of a cardiac strand with changing diameter or axial resistivity.[6 10-12] It was postulated that such a mechanism was responsible for the occurrence of UCB in isolated atrial preparations with a narrow isthmus bridging two large areas,[13 14] in the Purkinje-muscle junction,[15-17] and in the cell cultures with abrupt expansion.[18] In most cases, a high stimulation rate was applied to produce UCB. Because of this, additional factors including dispersion of refractoriness or the presence of a resistive barrier[10] could not be excluded.

The purpose of this study was to examine with microscopic resolution the changes in action potential wave shapes and the occurrence of UCB at a site of an abrupt tissue expansion. In particular, we tried to assess the critical width of a cell strand resulting in UCB without involvement of rapid pacing. The technique of patterned cell growth[19] was used to produce strands of neonatal rat myocytes of variable width emerging into a large cell area. Action potential upstrokes were recorded at high spatial and temporal resolution (distance 15 μm, sampling interval 10 μs) using the technique of multisite optical recording of transmembrane potential.[20 21] Changes in the action potential upstroke were related to local sodium current kinetics by means of a computer model for cardiac impulse propagation.

Part of this work has been published previously in abstract form.[22]

Methods

Preparation of patterned cell cultures and staining with voltage sensitive dye

Cell cultures – The method used to prepare patterned monolayers of heart cells has been reported elsewhere in detail.[19] In brief, cells were cultured on glass coverslips (22 mm diameter, 0.14 mm thickness, Haska, Switzerland) coated with photoresist KTFR (Kodak) which prevented the adhesion of myocytes. The specific growth pattern was etched in the photoresist using a photolithographic technique. Figure 1A shows the growth pattern used for our experiments. Regions free of photoresist formed parallel channels connecting large areas at

Department of Physiology, University of Berne, Bühlplatz 5, CH-3012, Berne, Switzerland: V G Fast, A G Kléber. Correspondence to Dr Fast.

the centre and at the periphery of the coverslip. The central area was 15.4 and 3.2 mm long in vertical and horizontal directions respectively. Two types of channels were present in the growth pattern mask with a width of 20-40 μm and 100-140 μm. The channel length was 3.5 mm.

Cell cultures were prepared from neonatal Wystar rats (two days old). Hearts from six to eight rats were collected, minced, and subjected to five or six cycles of serial dissociation steps in calcium and magnesium free Hanks balanced salt solution containing 0.1% trypsin, 60 $\mu g \cdot ml^{-1}$ pancreatin, 20 $units \cdot ml^{-1}$ penicillin, and 20 $\mu g \cdot ml^{-1}$ streptomycin at 35°C. The solutions obtained after each step (except the first) were sedimented by centrifugation, and the resulting cell pellets were resuspended in medium M199 (Gibco) having the following ionic composition (in $mmol \cdot litre^{-1}$): NaCl 137, KCl 5.4, $CaCl_2$ 1.3, $MgSO_4$ 0.8, $NaHCO_3$ 4.2, KH_2PO_4 0.5, NaH_2PO_4 0.3, with 20 $units \cdot ml^{-1}$ penicillin, 20 $\mu g \cdot ml^{-1}$ vitamin B-12, and 10% neonatal calf serum. The non-myocyte content of the cell suspension was reduced by preplating (see[19] for details). After preplating, the myocytes remaining in suspension were counted with a haemocytometer and diluted to 3×10^5 $cells \cdot ml^{-1}$. Two millilitres of cell suspension were placed in a well containing the coated coverslip. The cultures were incubated in a cell medium M199 containing 5% serum at 37°C in a humidified atmosphere containing 1.5% CO_2. Medium changes were performed every second day. In spite of the preplating procedure, a small number of non-myocyte cells could remain in the cultures. Only those monolayers containing no non-myocyte cells at the transition region between a strand and a large area were selected for measurements. Measurements were made between the third and 14th day. It was previously shown that electrophysiological parameters do not change significantly between the second and the 17th day.[19]

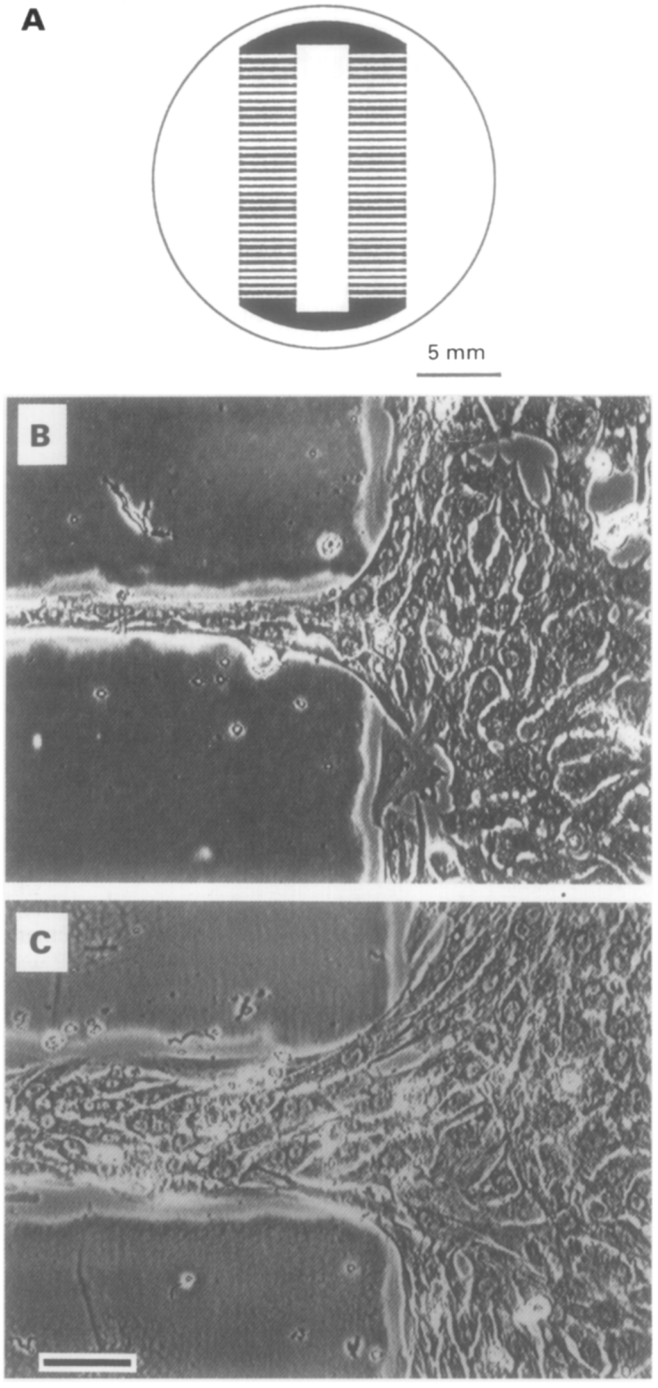

Figure 1 *(A) Photoresist pattern on circular glass coverslip used for cell cultures. Black areas depict photoresist coated regions where cells do not adhere. Non-coated, glass exposed regions (white), where cell growth takes place, consist of narrow (width 20-40 μm) and wide (width 100-140 μm) channels emerging abruptly into three large areas (lateral and middle white regions). (B) and (C): Phase contrast pictures of transition regions from narrow (panel B) and wide (panel C) strands emerging into a large area of a cultured monolayer of neonatal rat myocytes. Calibration bar = 50 μm.*

Staining – Coverslips were transferred into the experimental chamber mounted on a vibration-free table. Cells were superfused at a rate of 2 $ml \cdot min^{-1}$ with a solution of the following composition (in $mmol \cdot litre^{-1}$): NaCl 150, KCl 5, $CaCl_2$ 1.2, $MgCl_2$ 1, $NaHCO_3$ 5.8, Hepes 5, and glucose 5. pH was 7.4, and temperature was 34-35°C. The voltage sensitive styryl dye RH-237 (Molecular Probes) was used to measure transmembrane potential changes. The dye was stored in a 2 mM stock solution of dimethylsulphoxide (DMSO) and diluted to yield a final dye concentration of 2 μM in Tyrode solution (final DMSO concentration = 0.1%). Cells were superfused with the dye solution for 4-6 min.

Optical recording of transmembrane potential

Optical recording – An optical system as described previously[20 21] was used. The setup was built on an inverted microscope (Axiovert 35M, Zeiss) equipped for epifluorescence with a 100 W arc mercury lamp as a light source (fig 2). Fluorescence measurements were performed using a filter set with a bandpass exciting filter (530-585 nm), dichroic mirror (600 nm), and a low pass emitting filter (>615 nm). This combination of filters was better than the one used before,[20] yielding more fluorescent light and therefore a higher signal to noise ratio. An objective ×40 Plan-Neofluar, NA 1.3 Oil, (Zeiss) was used for optical measurements. Cells were briefly (50 ms) exposed to excitation light using an electromechanical shutter and shutter driver (UniBlitz VS25 and UniBlitz T132, Vincent Associates).

The fluorescence emitted by the dye was measured using a 10×10 photodiode array (Centronic) located in the image plan of the microscope. Individual photodiodes were squares with a diameter of 1.4 mm separated by a distance of 0.1 mm. The array covered a cell culture area of 150×150 μm^2. The centre to centre interdiode distance was 15 μm and an area of 14×14 μm^2 corresponded to each photodiode. The photocurrents from 96 diodes were fed into current-voltage converters built with operational amplifiers and 100 MΩ feedback resistors. After current-voltage conversion, 10 out of 96 channels were selected and directed into second stage amplifiers with a sample-and-hold circuit for subtraction of dc signals. These channels represented a horizontal row of 10 diodes in the middle of the array. Signals were sampled using three data acquisition cards; each card had four channels, 1 MHz throughput, and 12 bits resolution. The sampling rate was 100 kHz per channel. A personal computer was used for data storage and analysis. To eliminate high frequency noise, signals were digitally filtered using a gaussian low pass filter.[23] The cutoff frequency of 1.5 to 2 kHz was selected so that the filtration did not change the shape of the upstrokes. We have previously shown that errors introduced by this procedure are negligible.[20] The activation times were determined with two methods: first, from the moment of dF/dt_{max} where F is the optical signal, and, second, at the level of 50% change of optical upstroke ($F_{50\%}$). In order to characterise asymmetry between anterograde conduction (from a strand to a large area) and retrograde conduction (from a large area to a strand) across the site of geometrical transition, an average transitional velocity was defined as the ratio of the distance between two most distant diodes separated by 135 μm (centre to centre) and the difference in the respective activation times using the $F_{50\%}$ criterion. Anterograde and retrograde conduction were elicited by changing the location of the stimulation electrode. Repetitive exposures of cells to excitation light resulted in the slight reduction of dV/dt_{max} due to the phototoxic effect of the dye. To minimise effects of phototoxicity,[21] a given measuring site was exposed two times for 50 ms to excitation light. Impulse conduction was first measured in the direction from a strand to a large area and then in the reverse direction by changing the location of the stimulation electrode. Thus the occurrence of unidirectional conduction block was unaffected by phototoxicity. For analysis of directional differences in conduction

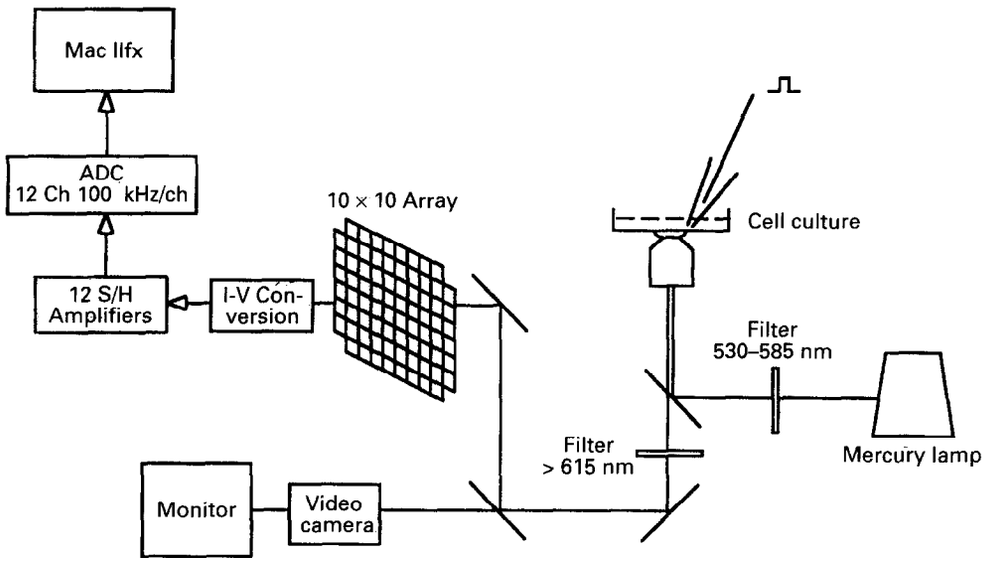

Figure 2 *Schematic diagram of the optical setup. See text for description.*

velocity, only the first two measurements with alternating direction of conduction were taken at a given site.

Electrical stimulation – Electrical stimulation was performed via a bipolar electrode composed of the conducting core of a glass pipette (tip diameter 50-70 μm) filled with the superfusion solution and a silver wire coiled around the pipette tip. Cells were stimulated with rectangular pulses (duration 1 ms, double threshold strength). To avoid the effect of stimulation rate on impulse conduction and conduction block, measurements were performed with long excitation intervals (>500 ms). Stimuli were delivered from an eight channel digital impulse generator (Master-8, AMPI). This generator was also used to synchronise the shutter opening and the data acquisition. To ensure that electrical stimulation did not interfere with propagation measurements, the stimulation electrode was placed >1 mm from the measurement site.

Morphology

Before each recording, cell morphology was observed in red light (filter >630 nm) and the photodiodes were positioned over a chosen area. Pictures showing the bright field illumination image of the cells and of the photodiodes and the phase contrast picture of cells were made by a video camera and a videographic printer. This procedure avoided phototoxic damage of cells.

Computer simulations of propagation

Computer simulations were performed on a 2-dimensional model representing a thin sheet of cardiac tissue. The extracellular medium was assumed to be isotropic and its resistance to be negligible. The surface to volume ratio was assumed to be constant throughout the medium. In contrast to our previous study,[20] intercellular and cytoplasmic resistances were lumped together and the model was considered to be internally continuous. The equation which describes propagation in such a model is the following:

$$c_m \frac{\partial V}{\partial t} = \frac{1}{S_v}\left[\frac{\partial}{\partial x}\left(\frac{1}{R_x}\frac{\partial V}{\partial x}\right) + \frac{\partial}{\partial y}\left(\frac{1}{R_y}\frac{\partial V}{\partial y}\right)\right] - I_{ion} \qquad (1)$$

where V = membrane potential, C_m = the specific membrane capacitance ($\mu F \cdot cm^{-2}$), S_v = a surface to volume ratio, I_{ion} = the total ionic current ($\mu A \cdot cm^{-2}$), and R_x and R_y = internal resistivities in x and y directions (Ω cm).

To solve equation (1) numerically, the model was divided into isopotential excitable patches with dimensions Δx and Δy. Substituting the right part of equation (1) with the difference approximation, the equation for the membrane potential of the patch with coordinates i,j is as follows:

$$c_m \frac{\partial V_{i,j}}{\partial t} = \frac{1}{S_v}[K_{x;i-1,j}(V_{i-1,j} - V_{i,j}) - K_{x;i,j}(V_{i,j} - V_{i+1,j}) + K_{y;i,j-1}(V_{i,j} - V_{i,j-1}) - K_{y;i,j}(V_{i,j} - V_{i,j+1})] - I_{ion} \qquad (2)$$

where $K_{x;i,j} = 1/\Delta x^2 R_{x;i,j}$ and $K_{y;i,j} = 1/\Delta y^2 R_{y;i,j}$, describing the resistive links in x and y directions of the element (i,j). The geometrical shape of the model and the pattern of the resistive connections were coded by coefficients $K_{x;i,j}$ and $K_{y;i,j}$ which were calculated in advance and stored in arrays. Impermeable boundary conditions were imposed on the borders of the medium ($K_{x;i,j} = 0$, $K_{y;i,j} = 0$). The geometry of the medium was defined by a thin strand (length 3 mm, variable width) abruptly emerging into a large area (length 3 mm, width 2 mm). The length of the strand as well as the dimensions of the large area were selected to ensure that impulse conduction at the transition region was unaffected.

Equation (2) was solved by the alternating direction implicit algorithm.[24] Space integration steps Δx, and Δy were 15 μm to ensure that the ratio between electrotonic space constant and the integration step was above 20. The ordinary differential equations for the ionic variables were solved by a simplifying algorithm[25 26] with the time integration steps of 2 μs. To calculate rate constants, computer generated lookup tables with $\Delta V = 0.1$ mV were used. The value for $C_m = 1.0$ $\mu F \cdot cm^{-2}$ was used in all calculations. The surface to volume ratio S_v was 0.67 μm^{-1}. The Beeler-Reuter model for ionic current I_{ion}[27] with the Ebihara-Johnson modification of fast sodium current kinetics[28] was used in this study. To provide for the high value of the maximum upstroke rate of rise measured in rat heart cell cultures, the value for the maximum sodium conductance was increased from 23 (original formulation of Ebihara-Johnson model) to 35 $mS \cdot cm^{-2}$. The reversal potential for the slow inward current was fixed at +70 mV. The value of R_i was varied to simulate the differences in conduction velocity between the strand and the large area. At a typical R_i value of 400 Ω cm, the conduction velocity was 33 $cm \cdot s^{-1}$ and the maximum upstroke rate of rise was 187 $V \cdot s^{-1}$ during uniform propagation of a rectilinear front. The membrane resistance, R_m, as measured with uniform current injection (space-clump), was 4642 Ω cm^2. The one-dimensional electrotonic space constant, $(R_m/S_v R_i)^{1/2}$, was 420 μm. These parameters were close to the values measured in cultured cell strands.[19 20 29] The electrotonic current, i_e, flowing into or from a given site was calculated from the first member of the right part of equation (1): $i_e = (\partial^2 V/\partial x^2 + \partial^2 V/\partial y^2)/S_v R_i$ in uniform case where $R_x = R_y = R_i$. According to equation (1), the current determining the shape of the action potential upstroke, $c_m \partial V/\partial t$, is the sum of the electrotonic current, i_e, and the ionic current, I_{ion}. Simulations were programmed in FORTRAN and carried out on a VAX-6410 computer with vector processor.

Statistical data are expressed as mean(SD). A two tailed non-paired Student's *t* test was used for comparisons. The investigation conforms with the *Guide for the care and use of laboratory animals* published by the US National Institutes of Health (NIH publication No 85-23, revised 1985).

Results

Seventeen individual dishes from eight cultures were used for the experiments. To characterise steady state conduction, velocity was measured inside of 19 strands and in eight cases in the large area. Changes in action potential waveform related to the abrupt expansion were measured in both anterograde (from a strand to a large area) and retrograde (from the large area to the strand) directions in 16 narrow and 10 wide strands. In the wide strands no conduction block was observed. Unidirectional conduction block was recorded in 7 of 16 narrow strands: a single impulse was reproducibly

blocked in anterograde direction while it passed in the retrograde direction.

Conduction within a strand and within a large area
Inside the strands, the average conduction velocity was 34.0(SD 6) $cm \cdot s^{-1}$ (n = 19). Inside the large area, the conduction velocity was less than in the strands: 25.6(4) $cm \cdot s^{-1}$ (n = 8, P < 0.005). These values compare well with our previous measurements in cell strands[20] or in isotropic cell monolayers.[21] The faster conduction in the strands is likely to be explained by the fact that the cells in a strand were elongated along the strand while cells were shorter in the large area.[19 21] Because of the elongated cell shape, the density of high resistance intercellular contacts per unit length is lower in the strand as compared to the large area. Therefore an average longitudinal intracellular resistance in strands is expected to be lower than in the large area, which could explain differences in conduction velocity. A similar explanation was proposed independently in a recent study.[30]

Impulse conduction at an abrupt expansion
Morphology of the transition region – The basic morphological features of the transition region between a strand and a large area are depicted on fig 1. Cell strands were 24(10) μm (1-3 cells in width) in narrow channels (n = 16) (panel B) and 93(16) μm (4-7 cells in width) in wide channels (n = 10) (panel C). Inside the strands, cells were elongated and orientated along the channel. Cell shapes gradually changed during the transition into a large area. In the large area, cells were polymorphic, ranging from almost polygonal or round to elongated. No preferential direction of cell orientation was observed. Before the transition the width of the strands gradually increased (funnel structure[15]) and this was especially evident in narrow strands (panel B).

Anterograde conduction – Panels A and B on fig 3 show a typical example of anterograde impulse propagation across the expansion region. A scheme (bottom right panel) shows the outline of transition region and the projection of the recording photodiodes. Along the strand, the strand width was about 22 μm (two cells in cross section). Immediately before the transition, the strand width increased gradually to 70 μm. The photodiode array was positioned in longitudinal direction over the transition area. Panel A depicts the recordings of action potential upstrokes (ΔF_n) at the corresponding sites, and panel B shows the first time derivatives (dF/dt) of all signals. Since the optical recordings do not provide absolute values for transmembrane voltage it was not possible to compare differences in the action potential amplitudes or the differences in voltage derivatives recorded from different sites. Hence both optical upstrokes and their derivatives were normalised and only changes in wave shapes were analysed. It can be seen that the configuration of action potential upstroke gradually changed when impulse passed through the transition. All upstrokes had two rising phases, which appeared on the derivatives (panel B) as two maxima. At points just proximal to the transition (points 1-4), a "hump" was observed after the initial rapid rise of potential. On the derivative traces this phase corresponded to a relatively small maximum after the initial large one. At the points distal to the transition (points 6-10) the phase with a rapid rise was preceded by a slow phase (the small initial maximum on derivative traces of panel B). At the intermediate location (number 5), the two phases had an almost equal rate of rise. The sequence of times of dF/dt_{max} (panel E, quadrangles) was discontinuous: at the first five diode locations (numbers 1-5) it occurred within a narrow time interval (160 μs). Between diodes 5 and 6, moments of dF/dt_{max} were 1700 μs apart. At the remaining diodes (numbers 6-10) dF/dt_{max} occurred again within a narrow interval (80 μs). The time sequence of $F_{50\%}$ (circles) was different. It was monotone and differed significantly from dF/dt_{max} over a distance of approximately 60 μm (four diodes). The average conduction velocity measured along 10 diodes (135 μm) was 8.9 $cm \cdot s^{-1}$ ($F_{50\%}$ criterion). From all the measurements, the velocity of anterograde conduction as defined from $F_{50\%}$ sequences was 11.1(3) $cm \cdot s^{-1}$ in narrow channels (n = 9) and 19.6(6) $cm \cdot s^{-1}$ in wide channels (n = 10, P < 0.002).

Retrograde conduction – Panels C and D on fig 3 show the retrograde conduction measured at the same site. For this measurement, the stimulation electrode was shifted to the large area. The action potential upstrokes at the transition region were monophasic (panel C) and the derivatives had only one maximum (panel D). Differences between moments of dF/dt_{max} and $F_{50\%}$ were minor. The average conduction velocity through the transition area was 80 $cm \cdot s^{-1}$. During retrograde conduction, the time interval between the peaks of dF/dt at locations 6 and 5 was much shorter than during anterograde propagation (30 μs *v* 1700 μs). This comparison indicates that the abrupt expansion of the tissue was the major determinant of anterograde conduction delays and excludes impaired electrical cell to cell coupling as a major cause.

The average velocity of retrograde conduction was 48.0(23) $cm \cdot s^{-1}$ (n = 8) and 40.1(6) $cm \cdot s^{-1}$ (n = 8) for narrow and wide channels respectively (difference statistically not significant).

Multiphasic waveshape – The biphasic waveshape of action potential upstroke, as shown on fig 3, was observed in all wide and in six out of nine narrow strands. In three out of nine narrow strands the upstrokes during anterograde conduction had three distinct phases. An example of impulse conduction in such a strand is shown on fig 4. The three rising phases (panel A) correspond to the three maxima on the derivative traces (panel B). The sequence of dF/dt_{max} times (panel C) shows that there were two sites with long delays: between diodes numbers 2 and 3 and between diodes numbers 9 and 10. As in the previous case, these delays were absent on the activation sequences defined by $F_{50\%}$. Measurement of retrograde conduction in these experiments revealed biphasic upstrokes. A local delay in the dF/dt_{max} sequence was observed at one of the two locations where delays were present during anterograde conduction. No differences in cell arrangement were found between these cultures and those showing only two rising phases. Most probably, the extra phase was related to local decrease of intercellular coupling.

Computer simulation of impulse conduction
Because of the non-uniform propagation and the multiphasic shape of the action potential upstrokes at the region of abrupt tissue expansion, the determination of local activation times was not straightforward. In particular, there was a large difference in activation times determined with the two different criteria dF/dt_{max} and $F_{50\%}$. Since the process of local activation in ventricular myocardium is basically determined by the flow of inward sodium current we used a computer model to relate changes in the potential waveforms to the kinetics of local sodium current.

The simulated upstroke waveshapes were qualitatively similar to the measured optical signals. Figure 5 shows the results of computer simulations of impulse conduction in the

uniform isotropic model ($R_{ix} = R_{iy} = 400\ \Omega$ cm). It shows the changes in action potential waveforms V (panel A), the first time derivative dV/dt (panel B), sodium conductance gNa (panel C), and sodium current iNa (panel D), calculated at 11 points in the transition region depicted on the inset. The spacing between points was 30 μm. The action potential amplitude remained nearly constant during both anterograde and retrograde conduction. On panel A, the amplitude decreased from 98 mV at the point 1 to 90.6 mV at point 4. Beyond this point, the amplitude increased again to 95 mV at point 11. Thus the largest difference in amplitude of action potentials was 7.4 mV or 7.6%. As in experiments, the upstrokes had two rising phases during anterograde conduction, and the derivatives had two maxima. The dV/dt_{max} gradually decreased from 179 $V \cdot s^{-1}$ (point 1) to 46 $V \cdot s^{-1}$ (point 8) and gradually increased beyond the transition. The point of equal amplitude in dV/dt_{max} (point 8) was located in the large area at the distance of 60 μm from the boundary. This is in contrast to the experimental data presented on fig 3 where the transition point was on the boundary. The reason for this discrepancy is likely to be the small anatomical funnel in the cell culture, which is predicted to shift the point of equal amplitude in dV/dt_{max} towards the strand. The changes in sodium current (panel D) were opposite to the changes in dV/dt: the absolute value of iNa_{max} gradually increased from 426 $\mu A \cdot cm^{-2}$ (point 1) to 639 $\mu A \cdot cm^{-2}$ (point 6) and decreased beyond the transition. Thus the sodium current was larger at the sites where the dV/dt_{max} became smaller. A similar relationship between iNa_{max} and dV/dt_{max} was observed at the boundary of a one-dimensional cable.[31]

The relationship between time course of dV/dt and local currents is demonstrated on fig 6A. Panel A shows simulations of dV/dt, sodium current iNa, and the electrotonic current i_e (see Methods). It can be seen that the first peak of dV/dt was solely due to the increase of electrotonic current, while the sodium current was not yet

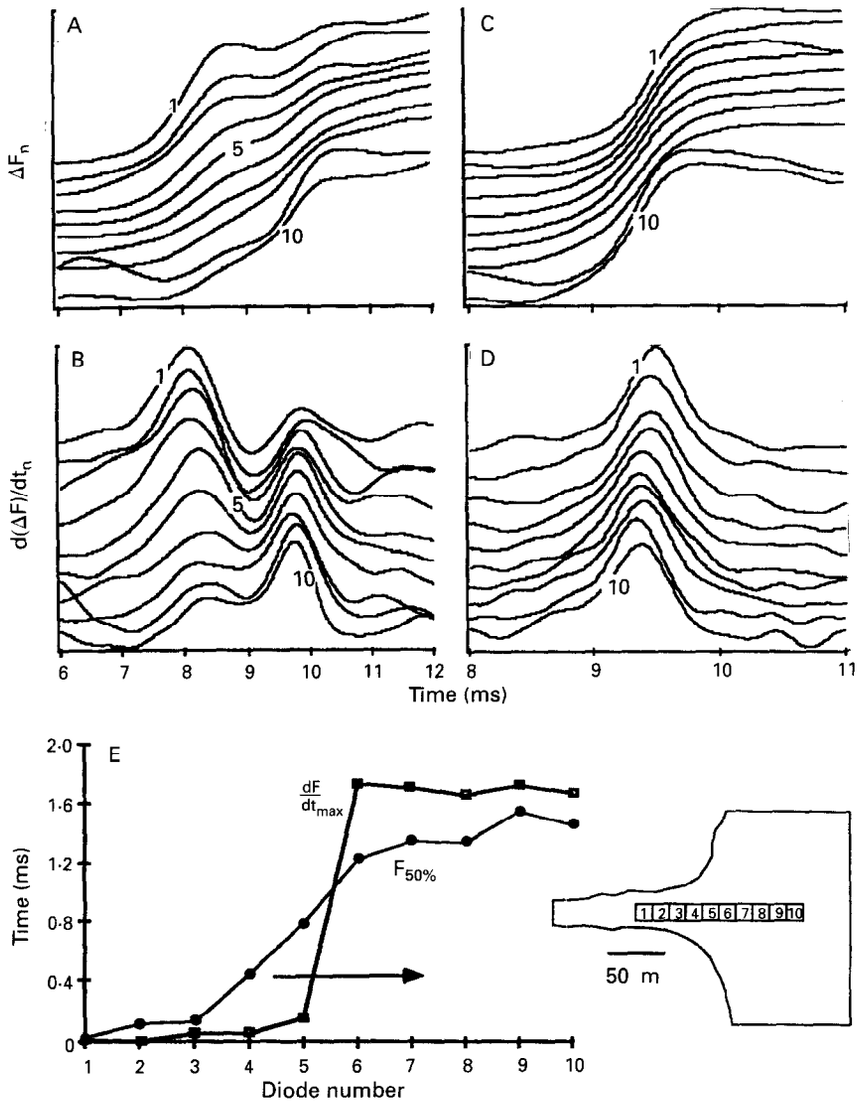

Figure 3 *Anterograde and retrograde impulse conduction at the region of abrupt expansion. Bottom right: Outline of the transition region. Strand width is 22 μm. The grid shows the localisation of photodiodes with numbers. An individual diode covers a cell membrane area of 14 × 14 μm^2. The spacing between borders of individual diodes is 1 μm. Panels (A) and (C): Normalised optical upstrokes (ΔF_n) recorded during anterograde conduction (A) from the strand into the large area and during retrograde conduction (C). Numbers on traces indicate corresponding photodiode numbers. Time was measured from the beginning of the recording interval. Stimulation pulse was delivered at t = 5 ms. Panels (B) and (D): Normalised first time derivatives of corresponding optical signals, dF/dt_n. Two rising phases can be seen on optical upstrokes ΔF_n corresponding to the two maxima on derivative traces dF/dt_n. Panel (E): Time sequences of dF/dt_{max} (quadrangles) and $F_{50\%}$ (circles) calculated from the recordings on panels (A) and (B). Data are plotted relative to the moment of dF/dt_{max} at the site number 1 which was considered to be zero.*

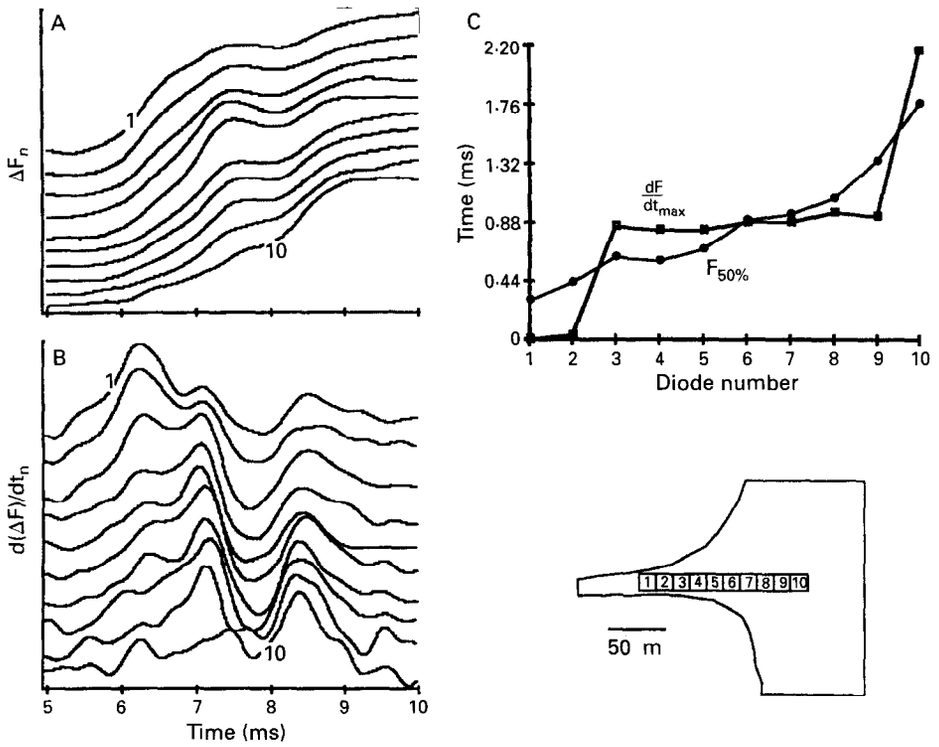

Figure 4 *Impulse conduction with multiphasic action potential upstrokes. Right bottom panel shows an outline of a strand (width 20 μm) emerging into a large area. Panel (A): Optical signals (ΔF_n) showing upstrokes with three rising phases. Panel (B): Corresponding derivatives dF/dt_n show three maxima. Time was measured from the beginning of the recording interval. Stimulation pulse was delivered at t = 4 ms. Panel (C): Time sequences of dF/dt_{max} (quadrangles) and $F_{50\%}$ (circles) calculated from the recordings on panels (A) and (B). Data are plotted relative to the moment of dF/dt_{max} at the site number 1 which was considered to be zero.*

activated. When iNa was activated, most of it was directed into the intracellular space for depolarisation of membrane surface downstream and not for local depolarisation. Therefore, in spite of the increase of sodium current, dV/dt decreased and reached a local minimum at a moment of iNa peak. dV/dt increased again when the electrotonic drain from

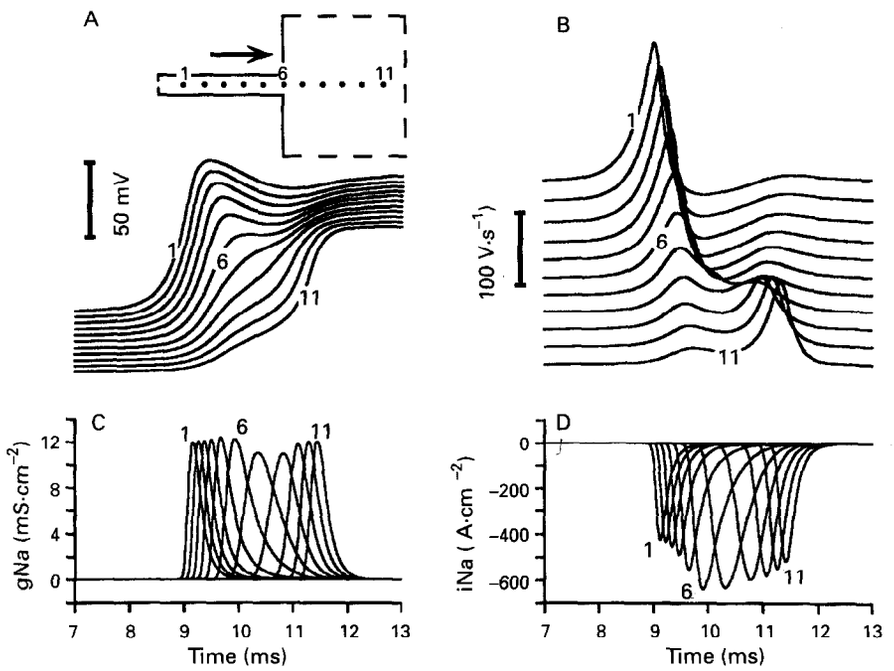

Figure 5 *Computer simulation of impulse conduction in a structure with abrupt expansion. Transmembrane action potentials V (panel A), first time derivative of action potential dV/dt (panel B), sodium conductance gNa (panel C), and sodium current iNa (panel D) calculated during impulse propagation from a narrow strand into a large area are shown. Time was measured from the onset of stimulus. The geometrical structure is indicated on the inset of panel A. The 11 recording points were 30 μm apart. The arrow indicates the direction of propagation. The strand width was 120 μm. The strand length was 3 mm (only a short strand portion is shown). The length and the width of the large area were 3 mm and 2 mm correspondingly.*

the downstream area decreased and more sodium current was available for local depolarisation. This reduction in electrotonic drain resulted in the second peak of dV/dt.

Panel B compares time sequences of three parameters: dV/dt_{max}, $diNa/dt_{max}$, and $V_{50\%}$. As in experiments, the sequence of dV/dt_{max} was discontinuous. Just before the transition point, the time delay of dV/dt_{max} between points 5 and 8 was extremely short: 130 μs on the distance of 90 μm. At the same time, the time delay was extremely large after the transition point. The longest delay was between points numbers 8 and 9, where the peaks of dV/dt were 1435 μs apart. In contrast to the sequence of dV/dt_{max}, the time sequence defined by the time of occurrence of $diNa/dt_{max}$ was smooth. When local activation was defined as the time of the 50% change of action potential amplitude ($V_{50\%}$), the activation sequence (dashed line) was also smooth and close to the sequence defined from the time of $diNa/dt_{max}$. Time sequences very similar to $V_{50\%}$ were obtained when activation times were defined as the time of the threshold level of sodium current or as the time of the maximal iNa (not shown).

The effect of a geometrical expansion on conduction velocity in the model was qualitatively similar to the experiments. The average velocity of anterograde conduction ($V_{50\%}$ criterion) measured over the distance of 150 μm in the transition area was smaller (9.3 $cm \cdot s^{-1}$) and retrograde velocity was larger (42.9 $cm \cdot s^{-1}$) than the steady state velocity in the strand (33.0 $cm \cdot s^{-1}$).

Effect of inhomogeneity in R_i – Morphologically, cell cultures were inhomogeneous: in the strands cells were elongated and orientated along the strands, while in the large area cells were shorter,[19 21] representing higher resistance to the current flow. As a result of a higher average axial resistivity, conduction velocity was smaller in the large area. To estimate the effect of the higher resistivity in the large area, this resistivity was increased both in x and y directions from 400 to 800 Ω cm. This resulted in a steady state velocity of 23.3 $cm \cdot s^{-1}$, which was close to the experimental data. Figure 7 shows the action potential waveforms at the transition region in this case. It can be seen that in spite of lower conduction velocity in the large area, conduction through the transition region was facilitated by the increase of the large area resistivity which was manifested in three parameters. First, the conduction was faster in the inhomogeneous model: the conduction delay between points numbers 1 and 11 decreased from 2260 μs (panel A) to 1655 μs (panel B). Second, the decrease in dV/dt_{max} related to the transition was smaller in the inhomogeneous model: minimum dV/dt_{max} at point number 8 increased from 46 $V \cdot s^{-1}$ (panel A) to 89 $V \cdot s^{-1}$ (panel B). Third, the biphasic shapes

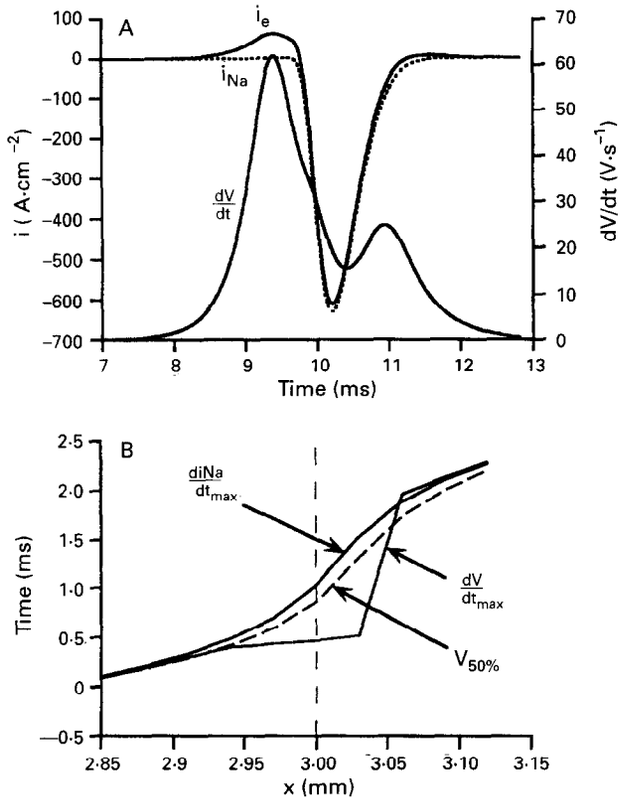

Figure 6 *Relationship between action potential upstroke and local ionic currents in the computer model. Panel (A): Superimposed tracings of action potential rate of rise (dV/dt), sodium current (iNa), and electrotonic current (i_e) flowing into or from a given site from surrounding area near the transition (point number 7 on fig 5) during anterograde conduction. Left y axis represents scaling for both sodium and electrotonic currents, right y axis represents scaling for voltage rate of rise. Time scale is the same as on fig 5. The dV/dt_{max} occurred long before the beginning of activation of sodium current, and the peak of iNa occurred near the local minimum of dV/dt_{max}. Panel (B): Time sequences of dV/dt_{max}, $diNa/dt_{max}$, and $V_{50\%}$. The dashed line marks the transition from the strand into the large area.*

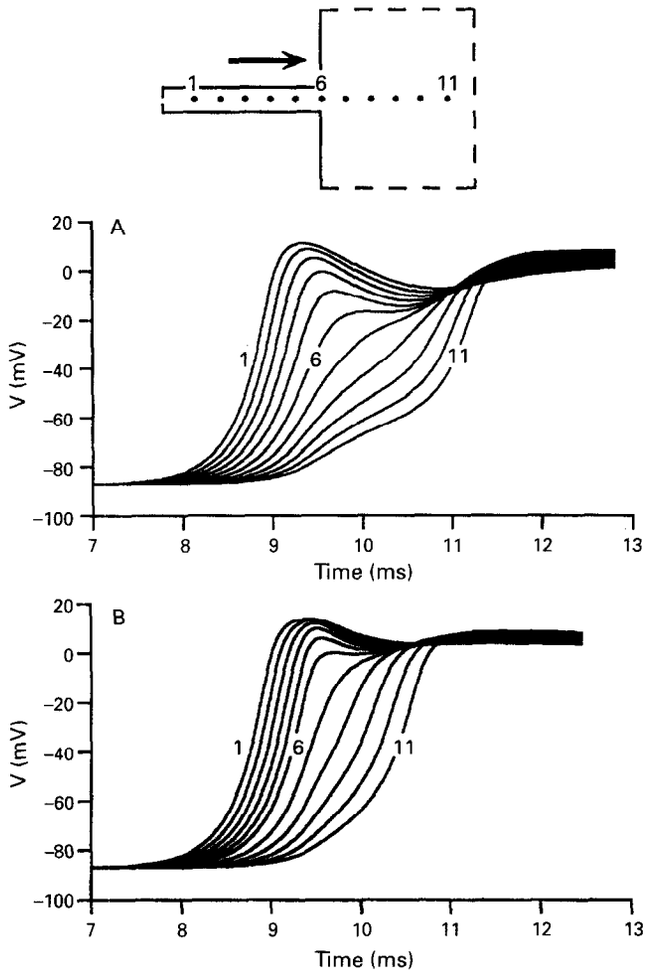

Figure 7 *Effect of increased resistivity in the large area on impulse conduction through the expansion region in the computer model. Panel (A): Action potential upstrokes in uniform model with $R_x = R_y = 400$ Ω cm. Panel (B): Resistivity in the large area increased from 400 to 800 Ω cm in both x and y directions. Time was measured from the onset of stimulus.*

of the upstrokes related to the geometrical expansion were less pronounced in the inhomogeneous model. The facilitation of conduction by the increase of the large area resistivity can be explained by the decrease of electrical load on the strand, similar to the effect of a resistive barrier in a one-dimensional model.[10] When the width of the strand was reduced, the biphasic upstroke waveshapes become pronounced again (not shown), resembling the control case. Therefore the increase in large area resistivity did not eliminate the conduction abnormalities completely but reduced the strand width at which they were observed.

There was a negligible effect (not shown) on conduction time and action potential wave shapes increasing transverse resistivity within the strand alone (transverse from 400 to 4000 Ω cm, to represent the 10-fold anisotropic ratio in resistivity known for myocardium[32]).

Unidirectional conduction block in cell cultures

Figure 8 shows an example of unidirectional conduction block in a narrow strand. Panels A and B show the upstrokes of optical signals recorded during anterograde and retrograde propagation. The location of the diodes within the geometrical expansion is depicted in the bottom panel. Signals on panel A are scaled with respect to the amplitudes of corresponding signals on panel B. During anterograde conduction, upstrokes were monophasic, that is, there was no second rising phase related to the activation of the large area. The amplitude of upstrokes gradually decreased, reflecting decremental conduction and eventual block. Independently from the optical recordings, conduction block was also confirmed visually from the lack of cell contractions in the large area, while cells in the strand were contracting. Since the amplitude of upstrokes decreased gradually, the determination of the exact location of the conduction block, that is, separation of small amplitude action potentials from purely subthreshold electrotonic impulses, was not possible. As an approximation, it was assumed that the conduction block occurred at a site where upstroke amplitude was less than 30% of its value during retrograde conduction. Such a level is close to the voltage threshold of the sodium current in the mathematical model. The point of last activation defined in such a way (diode number 7) was located just before the transition of the strand to the large area. During retrograde conduction (panel B), there was no slowing of

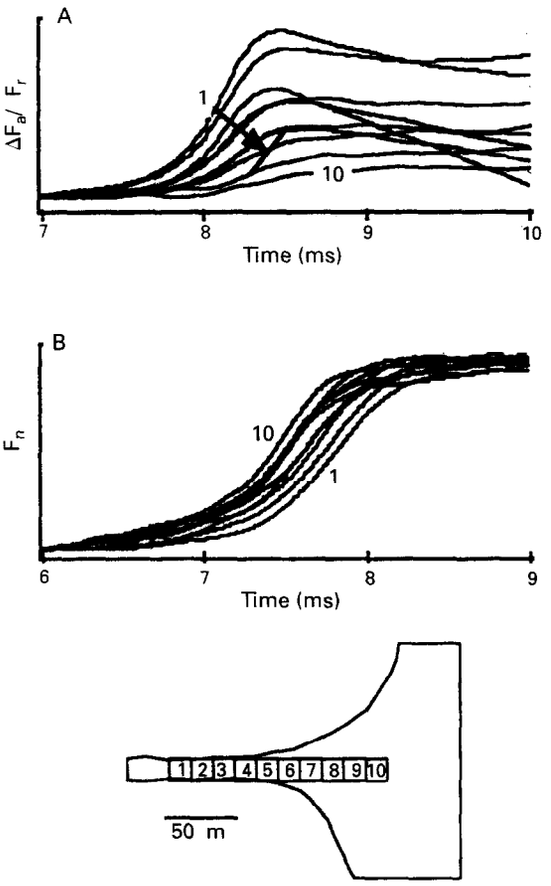

Figure 8 *Unidirectional conduction block in the cell culture. Bottom panel: The outline of the transition area with a strand of 15 μm in width. Panel (A): Optical recordings of action potential upstrokes showing conduction block in anterograde direction. Panel (B): Retrograde conduction. Time was measured from the beginning of the recording interval. Stimulation pulse was delivered at t = 5 ms. Signals on panel A are normalised with respect to their amplitudes during retrograde conduction shown on panel B. Arrow shows the direction of propagation. During anterograde propagation (panel A), the upstroke amplitude gradually decreased. The site of conduction block is between points numbers 7 and 8, if amplitudes less than 30% of normal are considered as electrotonic (see text). There was no slowing of conduction at this location in retrograde direction as shown on panel B.*

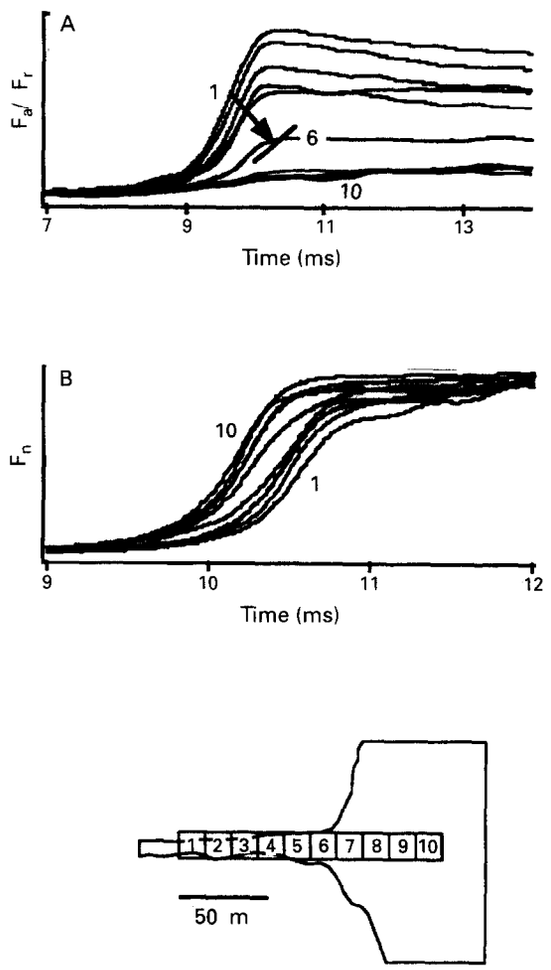

Figure 9 *Unidirectional conduction block in cell culture with local depression of conduction. Optical signals show conduction block in anterograde direction (panel A) and retrograde conduction (panel B). Time was measured from the beginning of the recording interval. Stimulation pulse was delivered at t = 5 ms. Bottom panel shows the outline of cell culture and localisation photodiodes. In anterograde direction, the upstroke amplitude decrease rapidly between points 5 and 6. There is local depression of conduction at this location during retrograde propagation.*

conduction at the point of anterograde block. The average velocity of retrograde conduction was 42.4(8) $cm \cdot s^{-1}$ (n = 5).

The pattern of conduction block described in fig 8 was observed in five out of seven cases. In two cases, anterograde conduction block was characterised by a more abrupt decrease of action potential amplitude and accompanied by local slowing of retrograde conduction. An example of this type of block is shown on fig 9. During anterograde propagation (panel A), the action potential amplitude vanished between points 5 and 6, and no subthreshold signals were detectable behind diode 6. During retrograde conduction (panel B), there was a delay in dV/dt_{max} between points 6 and 5 which amounted to 240 μs. The location of depressed retrograde conduction corresponded to the site of anterograde conduction block. Therefore it was concluded that in these two experiments a local decrease in excitability or cell to cell coupling contributed to the formation of block in addition to changing tissue geometry.

Unidirectional conduction block occurred in narrow strands with a width of 15(4) μm (n = 7) (1-2 cells in width). No conduction block was observed in narrow strands with a width of 31(8) μm (n = 9, $P < 0.001$) (2-3 cells in width) or in all wide strands. Thus the critical strand width for the occurrence of unidirectional conduction block in cell culture was 15 μm.

Discussion

This study was performed to examine impulse conduction at a cellular resolution in a region of abrupt tissue expansion and to relate local upstroke shape to ionic current flow in a computer model. Very thin cell strands were produced using the method of patterned cell growth, and the changes in action potential upstrokes were assessed at a high spatial resolution (15 μm) with an optical mapping of membrane potential. The following main findings were established. (1) Action potential upstrokes showed multiple phases during anterograde impulse conduction in the transition region which appeared as separate peaks on the first time derivative, dV/dt. At the site of the maximum decrement in conduction, these peaks were largely determined by the electrotonus and not by the inward sodium current. (2) Unidirectional conduction block occurred in narrow strands with a width of 15(SD 4) μm (1-2 cells). Action potential amplitude and activation times during retrograde propagation indicated that block was either due to expanding tissue geometry alone, or due to a combination of expanding geometry and local depression of conduction.

The rising phase of action potential and sodium current at a geometrical expansion

Since the experiments of Draper and Weidmann[33] and Weidmann[34] it has been generally accepted that the rapid depolarisation phase of the ventricular action potential is generated by the flow of inward sodium current. Subsequently a number of studies were concentrated on the relationship between the magnitude of the maximum upstroke rate of rise (dV/dt_{max}) and the peak sodium current (iNa). It is established that a monotone relationship exists between peak sodium current and dV/dt_{max} for space clamped (non-propagated) or uniformly propagated action potentials.[35] The relationship between dV/dt_{max} and iNa can be different in the case of non-uniform propagation. At the initiation site and at the boundary in a one-dimensional model, a larger sodium current corresponded to smaller dV/dt_{max} and vice versa.[31] Nevertheless, the rising phase of an action potential corresponded in time to the flow of sodium inward current, and the timing of dV/dt_{max} was relatively close to the peak sodium current or sodium conductance.[31]

Our findings indicate that there is no close correspondence between the upstroke rise and the flow of local inward sodium current at the site of an abrupt geometrical expansion. At points immediately adjacent to the transition, the peak of sodium current could occur at a time when dV/dt did not change. Thus, rising phases of upstrokes at these points were independent of the peak local inward current and reflected electrotonic interaction with surrounding tissue.

Determination of local activation at a geometrical expansion

The activation of ventricular cells is basically determined by the fast inward current. With microelectrode measurements the time of local activation is usually taken as the time of dV/dt_{max} of the action potential upstroke. Correspondingly, the time of the fastest negative or intrinsic deflection characterises local activation time in a unipolar extracellular electrogram. These estimates have been justified in case of uniform or slightly non-uniform conduction, when dV/dt_{max} coincides in time with the maximum rate of increase of gNA or iNa.[31 36]

The time sequence of dV/dt_{max} showed stepwise behaviour with a marked discontinuity at the transition point. At the same time, the time sequence of $diNa/dt_{max}$ was smooth and gradual. The differences between moments of dV/dt_{max} and $diNa/dt_{max}$ at the sites near the expansion could be rather large (~1 ms). Therefore the dV/dt_{max} activation criterion may give misleading results when used for calculation of conduction velocity in a tissue with abrupt expansion. However, dV/dt_{max} may be useful since it is a more sensitive indicator of the presence of changes in electrical load than $V_{50\%}$. Furthermore, the simulations showed that the time of half maximum amplitude, $V_{50\%}$, corresponded rather closely to the time of $diNa/dt_{max}$. Therefore, in the case of non-uniform propagation at the region of abrupt tissue expansion, $V_{50\%}$ appears to be a more reliable parameter for the time of local activation than dV/dt_{max}. The definition of activation times from extracellular electrograms at sites of changing tissue geometry is predicted to be more difficult, because multiple local deflections corresponding to the multiple phases of the action potential upstroke will be recorded in presence of continuous activation of local ionic currents.

Asymmetry of propagation at a geometrical expansion

Asymmetrical conduction occurred in all wide strands and in nine out of 16 narrow strands. The action potential upstrokes at the transitional region had a characteristic biphasic shape. Similar upstroke shapes have been reported in experiments on impulse transmission across Purkinje fibre-muscle junctions,[15 37] and in simulations of propagation in non-uniform one-dimensional cable models of axons[7 8] or cardiac strands.[10] Biphasic wave shapes were also reported in a recent independent study with an experimental preparation similar to ours.[18] Several mechanisms may potentially be responsible for the changes in action potential wave shapes, such as the abrupt change in tissue geometry, a local increase of axial resistivity, and a local dispersion of refractoriness. Several observations indicate that the change in tissue geometry alone was responsible for wave shape changes in majority of our experiments (all wide strands and six out of nine narrow strands). First, anterograde conduction was slowed with respect to the steady state conduction, while

conduction was accelerated in retrograde direction. This finding is predicted from the directional difference in electrical load, and it is not consistent with the presence of resistive barrier or a local depression of excitability. Second, the fact that the differences between the steady state, anterograde, and retrograde velocities were smaller in wide than in narrow strands further supports the dominating role of tissue geometry for the conduction changes. Third, biphasic action potential wave shapes in the anterograde direction and smooth continuous wave shapes in the retrograde direction indicate the absence of a local decrease in cell to cell coupling. In three narrow strands out of nine, where a triphasic action potential upstrokes were observed during anterograde conduction, biphasic upstrokes persisted during retrograde conduction. Most probably, this additional discontinuity in action potential upstroke was caused by the presence of a local resistive barrier.

Unidirectional conduction block at a geometrical expansion

Unidirectional conduction block has previously been demonstrated in a one-dimensional cable model with abruptly increased diameter, representing either an axon[7 8] or a cardiac strand.[6 10–12] The specific feature of the one-dimensional cable model is the existence of a critical *ratio* of diameters before and after the expansion region necessary for the occurrence of the conduction block. Critical ratios of 1:2 and 1:4 were reported for cardiac strands described by the Beeler-Reuter[10] and Ebihara-Johnson[12] ionic models, respectively. In contrast, in the two-dimensional model, conduction at the expansion region depended on the actual value of the strand width instead of a width ratio. Independent of the large area size, there is a unique value of strand width at which unidirectional conduction block occurs.

Rohr and Salzberg recently observed unidirectional conduction block in strands of cultured myocytes expanded to a large area at high pacing rates.[18] The high pacing rate (10 Hz) which was necessary for the occurrence of conduction block and the alternation of action potential duration near the transition region suggest that the relative refractoriness played a role in the block.

In our experiments, rate dependence was excluded by using long excitation intervals (>500 ms). Also, the experiments were designed in such a way that the dimensions of the large area did not play any role in the occurrence of the conduction block (the width of the large area was 15.4 mm, that is, many times greater than the electrotonic space constant of 360 μm[29]). In these conditions, conduction block occurred in strands with the width of 15(4) μm (one to two cells in width, n = 7). In a majority of cases, the retrograde conduction was uniform and fast, suggesting no significant local discontinuities in excitable or passive electrical properties. This leads to the conclusion that the small width of the strands was the main factor determining the occurrence of unidirectional block. No conduction block was observed in strands with the width of 31(8) μm. Therefore the critical strand width for the impulse conduction in cell monolayers was 15 μm. All narrow strands had a short expanding portion or funnel[15] immediately before the transition, which is supposed to have contributed to facilitation of anterograde impulse transmission. Therefore the critical strand size for a strictly abrupt expansion is expected to be somewhat larger than in cell monolayers. Rohr and Salzberg did not observe conduction block in strands with width of 40-80 μm during pacing at slow rates.[18] They concluded that conduction block was not possible with rectangular type of expansion. However, we believe that the absence of the rate independent conduction block in that study was related to the relatively large strand width. We also did not observe conduction block in strands with a width equal to or greater than 30 μm.

Relation to the adult myocardium

Unidirectional conduction block has been shown between a narrow isthmus and a large area of atrial tissue[13 14] and at the Purkinje fibre-muscle junction.[15–17] Usually, an intervention to depress the electrical driving force for propagation (premature stimulation or raised extracellular K^+) was required to produce conduction block.[13 15 16] The anatomical substrate for unidirectional conduction block can also be present in the border zone of infarcted myocardium where thin surviving strands of the infarcted region merge with healthy myocardium,[38] and a similar mechanism has been discussed to explain unidirectional block in atrioventricular accessory pathways.[14]

The present study is potentially useful for the estimate of the strand diameter critical for geometry dependent conduction block in heart tissue. Several factors, however, have to be taken into account before extrapolating our data to the situation of adult tissue. First, the properties of cultured cell monolayers are different from adult myocardium. The conduction velocity in our experiments was 26 $cm \cdot s^{-1}$ inside the monolayer and 34 $cm \cdot s^{-1}$ in the anisotropic strands. This is smaller than the longitudinal conduction velocity in myocardium (50-57 $cm \cdot s^{-1}$ [39–41]). This difference is in line with the electrotonic space constant of neonatal rat heart cell monolayers (360 μm),[29] which is smaller than the space constant measured in isolated adult cardiac tissue.[41 42] Therefore the critical strand diameter is expected to be larger in adult tissue than in cell cultures. A further argument for a difference between the cultured monolayers and adult myocardium relates to the three-dimensional structure of in vivo tissue. Because of higher electrotonic drain imposed by three-dimensional tissue, the critical strand diameter is expected to be larger in three than in two dimensions. Also, the presence of a small anatomical funnel in the cell cultures reduces the critical strand diameter to an extent which it is difficult to estimate quantitatively. Taking these three factors into account, the critical size in three-dimensional adult tissue is expected to be significantly larger than in two-dimensional cell cultures.

We wish to thank Dr Anne Gillis for reading our manuscript. We thank Mrs Regula Flückiger, Mrs Lilly Lehmann, Mr Denis de Limoges, Mr Hans-Ulrich Schweizer, and Mr Jürg Burkhalter for their technical assistance. This work was supported by the Swiss National Science Foundation and the Swiss Heart Foundation.

Key terms: ventricular myocytes; cell culture; action potential propagation; conduction block; voltage sensitive dyes; computer simulations.

Received 6 October 1994; accepted 3 January 1995. Time for primary review 29 days.

1 Allessie MA, Bonke FIM, Schopman FJC. Circus movement in rabbit atrial muscle as a mechanism of tachycardia. II. The role of nonuniform recovery of excitability in the occurrence of unidirectional block as studied with multiple microelectrodes. *Circ Res* 1976;**39**:168–77.

2 Gough WB, Mehra R, Restivo M, Zeiler RH, El-Sherif N. Reentrant ventricular arrhythmias in the late myocardial infarction period in the dog. 13. Correlation of activation and refractory maps. *Circ Res* 1985;**57**:432–42.

3 Fast VG, Pertsov AM. Shift and termination of functional reentry in isolated ventricular preparations with quinidine-induced inhomogeneity on refractory period. *J Cardiovasc Electrophysiol* 1992;**3:**255–65.

4 Downar E, Wasman MB. Depressed conduction and unidirectional conduction block in Purkinje fibers. In: Wellens HJJ, Lie KI, Janse MJ, eds. *The conduction system of the heart.* Philadelphia: Lea and Febiger, 1976:393–409.

5 Joyner RW. Mechanisms of unidirectional block in cardiac tissues. *Biophys J* 1981;**35:**113–25.

6 Sahakian AV, Myers GA, Maglaveras N. Unidirectional block in cardiac fibers – effects of discontinuities in coupling resistance and spatial changes in resting membrane potential in a computer simulation study. *IEEE Trans Biomed Eng* 1992;**39:**510–22.

7 Khodorov BI, Timin YN, Vilenkin SY, Gul'ko FB. Theoretical analysis of the mechanisms of conduction of a nerve pulse over an inhomogeneous axon. I. Conduction through a portion with increased diameter. *Biofizika* 1969;**14:**304–15.

8 Goldstein SS, Rall W. Changes of action potential shape and velocity for changing core conductor geometry. *Biophys J* 1974;**14:**731–57.

9 Swadlow H, Koscis J, Waxman S. Modulation of impulse conduction along the axonal tree. *Annu Rev Biophys Bioeng* 1980;**9:** 143–79.

10 Joyner RW, Veenstra R, Rawling D, Chorro A. Propagation through electrically coupled cells. Effects of a resistive barrier. *Biophys J* 1984;**45:**1017–25.

11 Henriquez CS, Plonsey R. Effects of resistive discontinuities of waveshape and velocity in a single cardiac fibre. *Med Biol Eng Comput* 1987;**25:**428–38.

12 Quan W, Rudy Y. Unidirectional block and reentry of cardiac excitation: a model study. *Circ Res* 1990;**66:**367–82.

13 De la Fuente D, Sasyniuk B, Moe GK. Conduction through a narrow isthmus in isolated canine atrial tissue. A model of the W-P-W syndrome. *Circulation* 1971;**44:**803–9.

14 Inoue H, Zipes DP. Conduction over an isthmus of atrial myocardium in vivo: a possible model of Wolf-Parkinson-White syndrome. *Circulation* 1987;**76:**637–47.

15 Mendez C, Mueller WJ, Urguiaga X. Propagation of impulses across the Purkinje fiber-muscle junctions in the dog heart. *Circ Res* 1970;**26:**135–50.

16 Sasyniuk BI, Mendez C. A mechanism for reentry in canine ventricular tissue. *Circ Res* 1971;**28:**3–15.

17 Overholt ED, Joyner RW, Veenstra RD, Rawling D, Wiedmann R. Unidirectional block between Purkinje and ventricular layers of papillary muscle. *Am J Physiol* 1984;**247:**H584–95.

18 Rohr S, Salzberg BM. Characterization of impulse propagation at the microscopic level across geometrically defined expansions of excitable tissue: multiple site optical recording of transmembrane voltage (MSORTV) in patterned growth heart cell cultures. *J Gen Physiol* 1994;**104:**287–309.

19 Rohr S, Schölly DM, Kléber AG. Patterned growth of neonatal rat heart cells in culture. Morphological and electrophysiological characterization. *Circ Res* 1991;**68:**114–30.

20 Fast VG, Kléber AG. Microscopic conduction in cultured strands of neonatal rat heart cells measured with voltage-sensitive dyes. *Circ Res* 1993;**73:**914–25.

21 Fast VG, Kléber AG. Anisotropic conduction in monolayers of neonatal rat heart cells cultured on collagen substrate. *Circ Res* 1994;**75:**591–5.

22 Fast V, Kléber AG. Tissue geometry as a determinant of unidirectional conduction block: assessment of microscopic excitation spread by optical mapping in patterned myocyte cultures. (Abstract) *Circulation* 1993;**88:**I–623.

23 Colquhoun D, Sigworth FJ. Fitting and statistical analysis of single-channel records. In: Sackman B, Neher E, eds. *Single-channel recording.* New York: Plenum Press, 1983: 191–263.

24 Peaceman DW, Rachford HH. The numerical solution of parabolic and elliptic differential equations. *J Soc Indust Appl Math* 1955; **3:**28–41.

25 Rush S, Larsen H. A practical algorithm for solving dynamic membrane equations. *IEEE Trans Biomed Eng* 1978;**BME-25:** 389–92.

26 Victorri B, Vinet A, Roberge FA, Drouhard J-P. Numerical integration in the reconstruction of cardiac action potentials using Hodgkin-Huxley-type models. *Comput Biomed Res* 1985;**18:** 10–23.

27 Beeler GW, Reuter H. Reconstruction of the action potential of ventricular myocardial fibres. *J Physiol (Lond)* 1977;**268:** 177–210.

28 Ebihara L, Johnson EA. Fast sodium current in cardiac muscle. A quantitative description. *Biophys J* 1980;**32:**779–90.

29 Jongsma HJ, van Rijn HE. Electrotonic spread of current in monolayer cultures of neonatal rat heart cells. *J Membr Biol* 1972;**9:**341–60.

30 Rohr S, Salzberg BM. Multiple site optical recording of transmembrane voltage (MSORTV) in patterned growth heart cell cultures: assessing electrical behavior, with microsecond resolution, on a cellular and subcellular scale. *Biophys J* 1994;**67:** 1303–15.

31 Spach MS, Kootsey JM. Relating the sodium current and conductance to the shape of transmembrane and extracellular potentials by simulation: effects of propagation boundaries. *IEEE Trans Biomed Eng* 1985;**BME-32:**743–55.

32 Clerc L. Directional differences of impulse spread in trabecular muscle from mammalian heart. *J Physiol (Lond)* 1976;**255:** 335–46.

33 Draper MH, Weidmann S. Cardiac resting and action potentials recorded with an intracellular electrode. *J Physiol (Lond)* 1951; **115:**74–94.

34 Weidmann S. The effect of the cardiac membrane potential on the rapid availability of the sodium-carrying system. *J Physiol (Lond)* 1955;**127:**213–24.

35 Walton MK, Fozzard HA. The conducted action potential: models and comparison to experiments. *Biophys J* 1983;**44:**9–26.

36 Rudy Y, Quan W. Propagation delays across cardiac gap junctions and their reflection in extracellular potentials: a simulation study. *J Cardiovasc Electrophysiol* 1991;**2:**299–315.

37 Bukauskas FF, Sakson MY, Kukushkin NI. Discrete zones of the electrical connexion of Purkinje terminals with muscle fibres in the canine ventricle. *Biofizika* 1976;**21:**887–92.

38 Smith JH, Green CR, Peters NS, Rothery S, Severs NJ. Altered patterns of gap junction distribution in ischemic heart disease – an immunohistochemical study of human myocardium using laser scanning confocal microscopy. *Am J Pathol* 1991;**139:**801–21.

39 Spach MS, Miller WTI, Gezelowitz DB, Barr RC, Kootsey JM, Johnson EA. The discontinuous nature of propagation in normal canine cardiac muscle. Evidence for recurrent discontinuities of intracellular resistance that affect the membrane currents. *Circ Res* 1981;**48:**39–54.

40 Roberts DE, Scher AM. Effect of tissue anisotropy on extracellular potential fields in canine myocardium in situ. *Circ Res* 1982;**50:**342–51.

41 Kléber AG, Riegger CB. Electrical constants of arterially perfused rabbit papillary muscle. *J Physiol (Lond)* 1987;**385:**307–24.

42 Weidmann S. Electrical constants of trabecular muscle from mammalian heart. *J Physiol (Lond)* 1970;**210:**1041–54.